energies

MDPI

Article

Distributed Secondary Control for Battery Management in a DC Microgrid

Alexander Paul Moya [1,*], Polo Josue Pazmiño [1,*], Jacqueline Rosario Llanos [1], Diego Ortiz-Villalba [1] and Claudio Burgos [2]

[1] Department of Electrical and Electronic Engineering, Universidad de las Fuerzas Armadas (ESPE), Sangolquí 171103, Ecuador
[2] Institute of Engineering Sciences, Universidad de O'Higgins, Rancagua 2820000, Chile
* Correspondence: apmoya1@espe.edu.ec (A.P.M.); pjpazmino@espe.edu.ec (P.J.P.)

Abstract: This research presents the design and simulation of a distributed secondary control based on a consensus algorithm for the efficient management of an isolated DC microgrid (MG-DC) that secures the distribution of active power according to the capacities of each storage unit, reducing duty cycles and extending its life cycle. The balance of powers is fulfilled through a photovoltaic (PV) generation unit and an energy storage system (ESS) based on batteries. The PV Boost converter has a maximum power point tracking (MPPT) controller based on the perturb and observe (P & O) method. In contrast, a Buck–Boost converter is integrated into each battery, which is bidirectionally controlled through a local controller and a primary droop control that balances the required power at the loads. It produces a voltage deviation on the DC bus. To compensate for this deviation, a distributed secondary control strategy based on consensus is proposed to restore the voltage while managing the power sharing according to the capacities of each battery. It allows for the improvement of its life cycle, which is shown in the state of charge (SOC) index, thus extending its life cycle. The controllers are evaluated for solar re-source changes, load changes, and different storage capacities.

Keywords: isolated DC microgrid; droop control; voltage restorer; distributed secondary control; consensus algorithm

Citation: Moya, A.P.; Pazmiño, P.J.; Llanos, J.R.; Ortiz-Villalba, D.; Burgos, C. Distributed Secondary Control for Battery Management in a DC Microgrid. *Energies* **2022**, *15*, 8769. https://doi.org/10.3390/en15228769

Academic Editors: Mahmoud Shahbazi and Sajad Sadr

Received: 4 October 2022
Accepted: 9 November 2022
Published: 21 November 2022

1. Introduction

Over the years, energy consumption has significantly increased worldwide, and the current needs facing energy supply involve a significant threat to the economic sector and sustainable development [1,2]. Therefore, new proposals for energy expansion have arisen to supply the demand, either based on fossil fuels or alternative energies [3,4].

In the last decade, a topic of interest at the societal level has been to decrease the use of fossil fuels by reducing the impact of carbon dioxide on the earth, which has led to the creation of power plants based on renewable energies [5]. The U.S. International Energy Agency forecasts that the use of clean energy resources will increase by 50% between 2019 and 2024 [6]. On the other hand, several places, such as rural areas, are affected by energy deficiency, highlighting aspects such as income level, social status, consumption level, and limited access to modern, clean, and sustainable energy. Approximately 777 million people in the world lack access to electricity, with 84% of these people correspond to geographically remote areas where the access to these territories is limited [7]. An environmentally friendly alternative that can be implemented in isolated areas are microgrids (MGs), allowing the incorporation of distributed generation sources based on renewable energies (RES). The use of this type of electrical system has a positive connotation in the reduction in environmental impact [8,9]. In general terms, an MG is a system that integrates distributed generation units (DG), usually from renewable or nonconventional sources such as solar cells, biogas, wind energy, and microturbines, among others, and supplying the demand to the load

in addition to energy storage systems (ESS) that are installed near the load. [1,10]. The generation units in an MG operate autonomously or are connected to the grid and are managed through an energy management system (EMS) to improve the system's stability involving technical and economic benefits [11]. The energy management system (EMS) is considered the coordinating unit of an MG since its work is controlling the energy flows between controllable components, i.e., generation units, loads, and storage elements, to support the MG's operation [9,12].

Microgrids can operate in DC, AC, and hybridized systems [13]. Both hybrid systems, as well as MG-DC, are gaining increasing interest in terms of efficiency and usability, offering advantages such as a) reduced losses and a higher efficiency due to the absence of reactive power and the reduction in rectifiers, b) direct current input, which is currently used by modern devices, c) no power factor losses, d) optimal control, or in other words, no reactive power or frequency controls are required, and e) high reliability due to its ability to operate remotely [14].

In recent years, solar energy has become one of the most applied renewable resources due to its unlimited potential and easy accessibility [15]. Research has contributed advances and efficient improvement in power distribution by photovoltaic panels; for example, [16–18] proposed the use of DC-DC converters with high voltage gain, soft switching capability, and high efficiency. These configurations minimize parasitic capacitance effects in the photovoltaic system. In addition, it facilitates the tracking of energy required from the PV source according to the load demand. It is worth mentioning that this research work implements conventional control strategies that can be adapted to the converters proposed in [16–18].

Batteries in microgrids with an isolated operation support the stability of the microgrid; their charge and discharge operation allow the continuous supply of energy towards the demand depending on their proper management [19]. Traditional EMSs usually do not consider features that allow the incorporation of the proper operation of the batteries where the life cycle of these systems is contemplated [20].

From the point of view of controllers focused on the storage management system, different solutions are proposed in the literature. In [11], a fuzzy logic control in an isolated microgrid is proposed, where its management strategy employs generation and load forecasts that provide the future action of the microgrid, where its primary objective is to extend the battery lifetime by predicting the excess of photovoltaic energy and dispensing this energy to avoid overloading the SOC, so that it oscillates at a value of 75% of its load. While a Takagi–Sugeno (TS) fuzzy controller approach is proposed by dividing the nonlinear system into local linear subsystems, by subsequently employing the fuzzy combination of the local rules, the general fuzzy model is obtained; this ensures the response is stable, reducing the MG oscillations with multiple constant power loads. The main problem with these techniques is that being knowledge-based, they require accurate information about the system operation. In [21], intelligent energy management that was control oriented in combined methods of fuzzy logic and a fractional-order proportional-integral-derivative (PID) controller (FO-PID) was proposed to adaptively adjust its gains, increasing its robustness considerably and improving the quality of the energy distributed to the MG-DC by regulating its reactive power and the DC bus voltage. In [22], an adaptive control method for MG-DC applications was proposed that satisfies both the current distribution and good voltage regulation, depending on the load condition, i.e., the load is directly proportional to the output current of the generation units, thus seeking to share the current accurately.

In [23], a two-level voltage and power drop control method was presented for the distribution of adequate power and voltage in the DC bus, which produces voltage deviations that increase with high loads. To solve this problem and improve its stability, the authors proposed a secondary control that is responsible for restoring the voltage derivative. Note that these control strategies use a centralized control architecture, which can produce that against the disconnection of a generation unit, and the power distribution can present devi-

ations. On the other hand, [24,25], based on the virtual voltage drop parameter, presented a new distributed secondary control strategy with event-triggered signal transmissions, ensuring current sharing as well as voltage regulation on the bus, and the charging and discharging management of the batteries with a renewable energy source was not analyzed.

Reference [26] presented the SOC-based adaptive droop control in an MG-DC, which is responsible for balancing the state of charge in each energy storage unit, while [27] used a dual-quadrant state-of-load (SOC)-based adaptive control strategy to extend the lifetime of distributed energy storage units (DESUs); these proposals are based on decentralized architecture and require a tuning parameter to adjust the SoC-balancing speed. On the other hand, [28,29] provided an analysis and classification of the control structure and the topology of DC-DC converters, whereby different control methods were applied to an MG-DC, mainly for the primary and secondary level of hierarchical control, to study important points and evaluate them critically. In the control strategies described above, although voltage restoration was proposed and droop control was used as a control strategy, the active power sharing was not analyzed according to its capabilities.

This research proposes a control scheme for managing an isolated MG-DC composed of a photovoltaic system that takes advantage of the solar resource generated during the day and two batteries with different energy storage capacities that store the energy generated by the photovoltaic module. The units in the MG-DC are connected to the DC bus along with a DC load. The PV system is connected to the bus via a Boost configuration converter, which uses an MPPT based on the perturb and observe (P & O) method. On the other hand, the storage system consisting of two batteries is connected to the load in parallel with a bidirectional Buck–Boost topology converter. The batteries are controlled by three levels of control. The first one corresponds to the local PI cascaded voltage and current controllers. The second one corresponds to a primary voltage droop controller, which guarantees battery power sharing. Finally, secondary control is proposed to efficiently correct the voltage deviation caused by the primary control and share power. The designed controllers are validated for different radiation scenarios, different capacities of the storage units, and load changes. The performance of each control level is analyzed.

The main contribution of this work is to propose a battery management strategy that prolongs their life cycle through the correct distribution of power, respecting their capacities, and ensuring a constant nominal voltage on the DC bus. The traditional droop control techniques allow the power sharing. However, there is a voltage deviation in the MG, for which the conventional secondary control supports in its compensation, but at the same time, they can cause the power sharing to be affected, making the batteries of a lower capacity degrade rapidly. Therefore, a consensus-based distributed secondary control is proposed to guarantee the nominal voltage in the MG-DC without affecting the efficient power sharing between the units in the face of load and irradiance changes.

2. System Description

The isolated direct current microgrid (MG-DC) shown in Figure 1 is composed of a photovoltaic (PV) panel and two energy storage units, with different capacities, connected to a DC bus through converters arranged for different configurations, either an unidirectional Boost-type converter for the PV or a bidirectional Buck–Boost topology for the storage units, where the power converters coupled to the MG-DC can stabilize a voltage of 48 V on the DC bus. The DG unit, which is the PV array, oversees injecting energy both to supply the demand and to provide the ESSs that enter a continuous state of charge when there is a power surplus.

The photovoltaic (PV) panel comprises a combination of solar cells in series and parallel, which distribute the required voltage and current under normal conditions. The current and voltage properties of a solar panel are nonlinear and depend on the solar radiation, and for a set amount of solar radiation, there is a maximum power point corresponding to the voltage at which the PV can provide its maximum energy. This study uses a disturb

and observe method for MPPT control [30]. The general scheme of the proposed controller is shown in Figure 2.

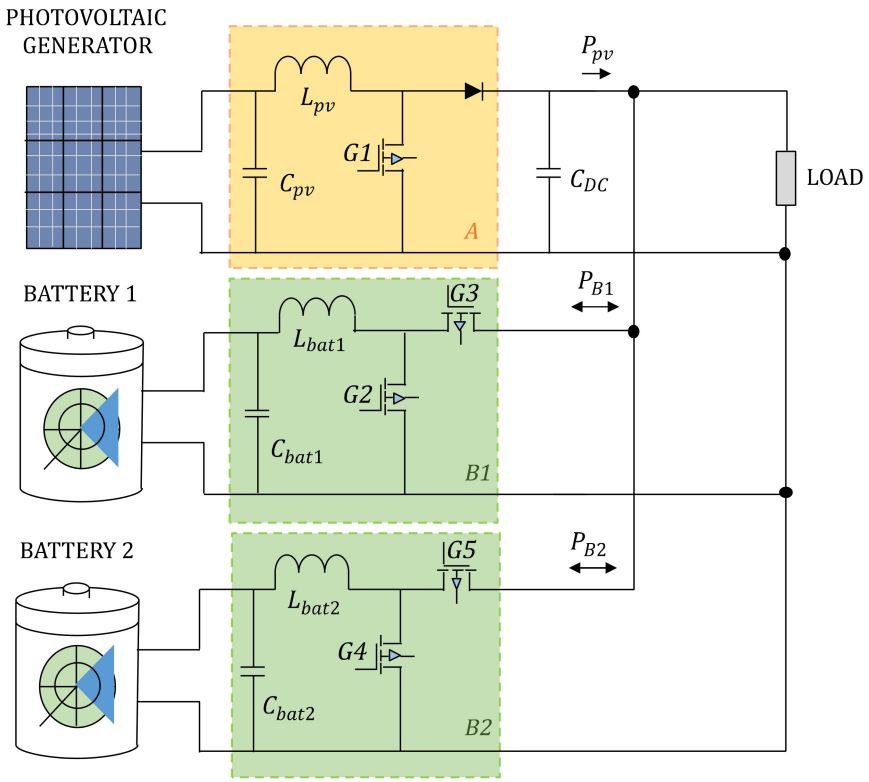

Figure 1. Schematic of an isolated DC microgrid.

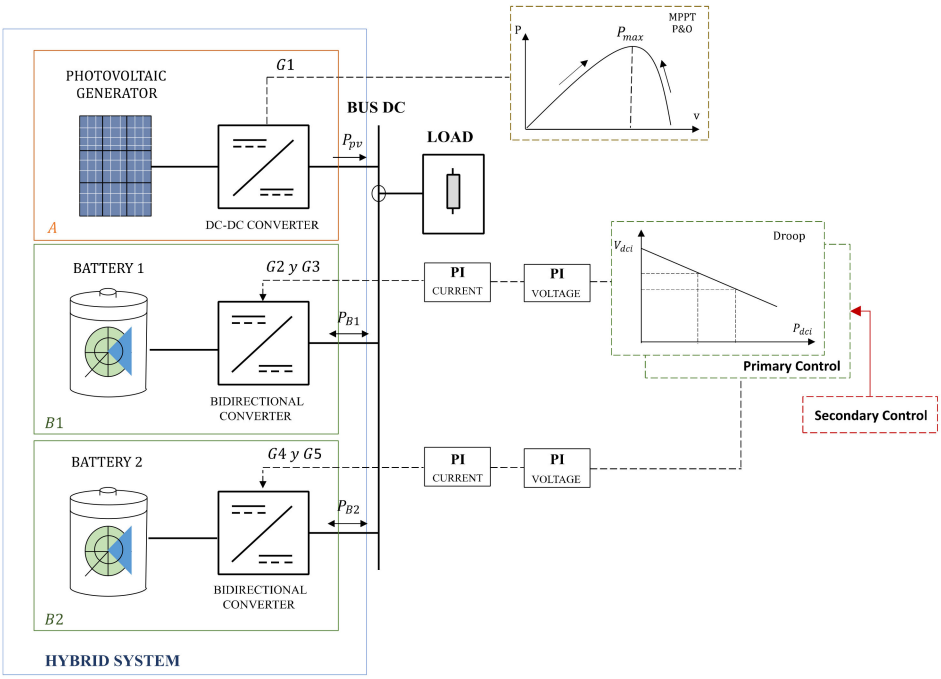

Figure 2. Configuration diagram of an MG-DC.

In this research, the storage system was assembled by two lead acid electrochemical batteries. They are the most used batteries in stationary applications, due to their operation

in a wide temperature range and low cost. The batteries work in two modes of operation: charge and discharge; the discharge is performed at a constant current, causing a decrease in voltage and taking positive values in power, while the charge mode is the opposite. This is shown in the state of charge (SOC). The SOC represents the energy stored in a battery and is expressed as a percentage between 0% and 100%. The preservation of battery life measured in cycles can be achieved through the behavior of the SOC, i.e., the number of times the battery operates in its two modes (charge and discharge). Consequently, the battery decreases its properties in each cycle, i.e., the more cycles there are, the faster its degradation accelerates.

In this research, three control architectures were designed and evaluated: the first one was a local voltage and current control, the second one was a primary control based on voltage drop, and the third one was a distributed control based on a consensus algorithm that encompassed voltage restoration and power compensation; the configuration diagram of an MG-DC is visualized in Figure 2.

3. Design of System Control Strategies

This section describes the control levels implemented in the system, as shown in Figure 3. At the bottom are the local controllers; in the case of the solar panels, they are responsible for making the most of the natural resources to generate power that will be used to supply the demand and the power required to charge the batteries. In the case of the batteries, the controllers allow operation in charge and discharge mode. A voltage droop control is included for the power sharing. The primary control produces voltage deviations in the MG, which can be corrected by a secondary control level, where the energy management system has been included for the operation of the batteries considering their storage capacities. The distributed control architecture based on voltage restoration and power compensation is designed and analyzed in this research work. It is important to note that the batteries are managed as dispatchable units for the energy management system, while the PV power is considered input to the management system. The description of each level of control is detailed in the following sections.

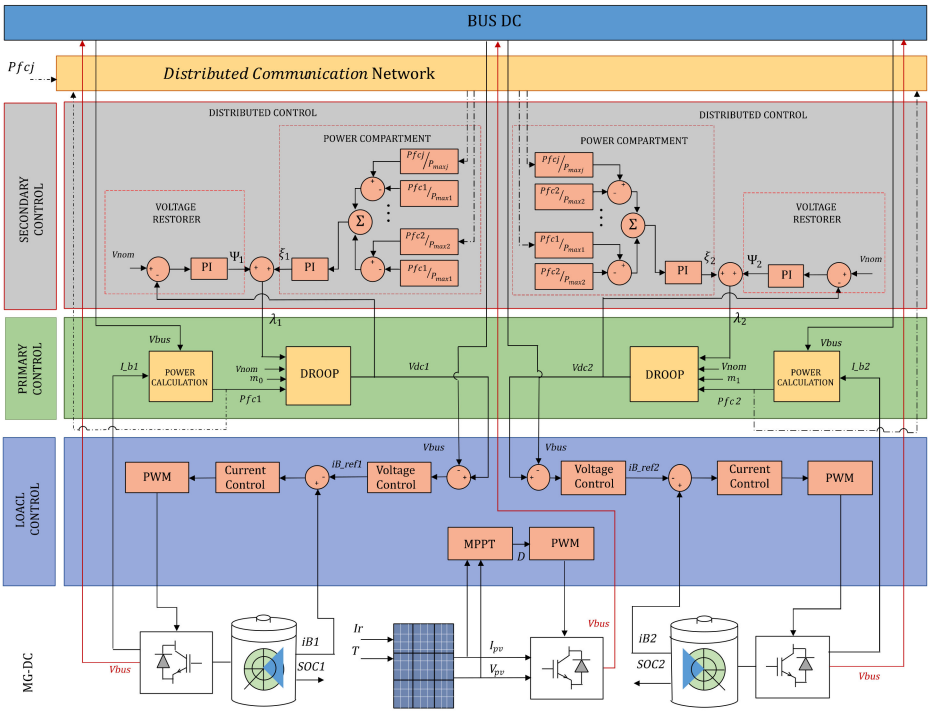

Figure 3. Control architecture.

3.1. Design of Local Controllers

3.1.1. Design of an MPPT Control Strategy for the Photovoltaic Panel

In this section, the photovoltaic panel controller algorithm is designed (Figure 1). The control objective is to maximize the solar resource using an MPPT control based on the perturb and observe (P & O) technique [31]. The implementation of the controller is shown in Figure 3, where the duty cycle (D) is obtained from the algorithm described in Figure 4, sending this signal to the PWM that controls the converter.

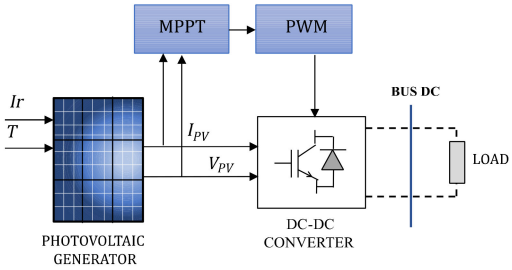

Figure 4. MPPT control for PV.

Figure 5 consists of comparing the PV voltage (V_{pv}) and PV power (P_{pv}) with those obtained at a previous instant $P_{pv}(k-1)$ and $V_{pv}(k-1)$. The instantaneous power is calculated by Equation (1) where (I_{pv}) represents the PV current. It is worth mentioning that, depending on irradiance and temperature, the maximum power point may oscillate, considering that these physical conditions are not constant and fluctuate significantly.

$$P_{pv}(k) = V_{pv}(k) \cdot I_{pv}(k) \tag{1}$$

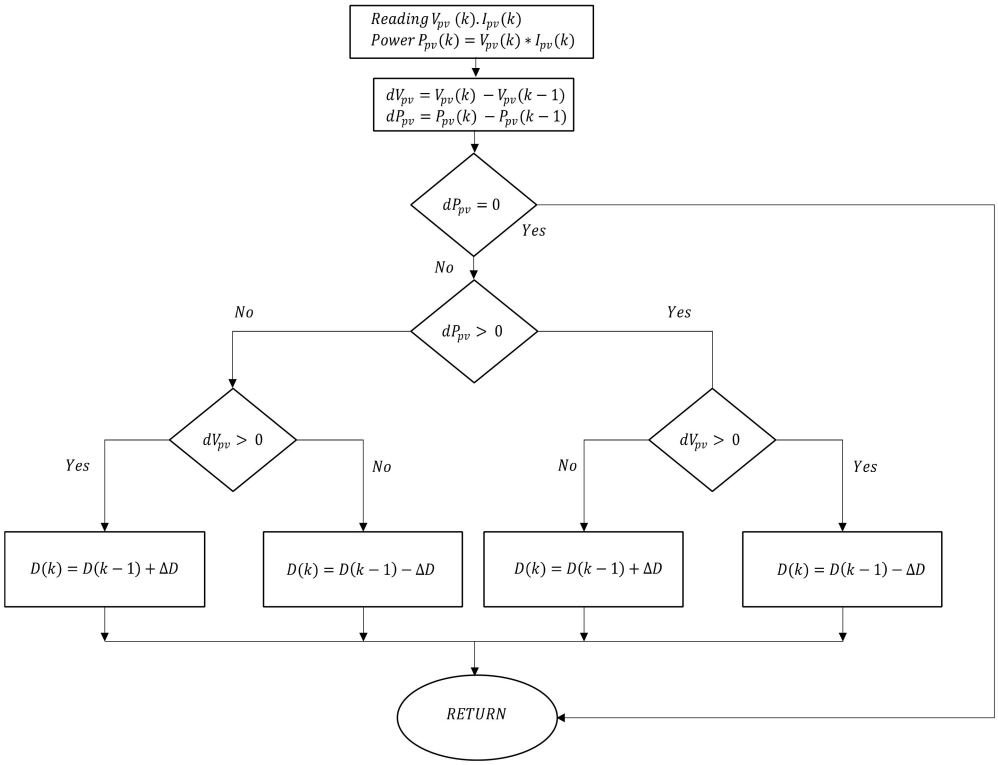

Figure 5. Flow chart for PV control.

Subsequently, the conditions entered in the flow diagram of Figure 5 are checked. If the power $P_{pv}(k)$ is greater than that obtained in a previous instant $P_{pv}(k-1)$, the direction

of the perturbation (Δ) around the duty cycle is maintained $D(k)$; otherwise, it will change direction; its equation can be represented as (2):

$$D(k) = D(k-1) + \Delta D \tag{2}$$

Figure 5 shows the algorithm flowchart, which is based on obtaining the voltage and current for the power calculation. A voltage and a current power minus a previous sample are evaluated. When a power difference equal to zero is achieved, the maximum power point will be reached; otherwise, we have to evaluate the values in the voltage difference to modify the behavior of the disturbance (ΔD) for both its decrease and increase to achieve the maximum power point.

3.1.2. Design of a Local Control Strategy for the Storage System

The control of the storage systems determines the appropriate duty cycle for the converters shown in Figure 1B1,B2, where there are two modes of operation, either Buck for battery charging and Boost for discharge. This change can be shown in the voltage of each battery. If the voltage is reduced, the battery is discharged, and the duty cycle of the converter increases as the system requires energy to regulate the nominal voltage on the DC bus. Conversely, when there is excess power from the PV, the batteries are charged, increasing the voltage and reducing their duty cycle. This is achieved by controlling the PWM signal of gates $G2$ and $G3$ for battery 1, and $G4$ and $G5$ for battery 2 (Figure 1). Figure 6 shows the block diagram of the controllers for B1 and B2, where two proportional and integral (PI) control loops are identified: an external one to control the battery voltage keeping the bus at a reference value, and the internal current control that defines the operation mode of the batteries for both charging and discharging. V_{dci} represents the output of the droop controller, V_{bus} represents the reference voltage on the DC bus, iB_ref_i represents the reference current output of the PI control, iB_i represents the battery current, and i represents the storage unit. $G3$ or $G5$ represents the trip to the converters when it is in charge mode (Buck); on the other hand, $G2$ or $G4$ represents the opposite action, meaning the converter is in discharge mode (Boost).

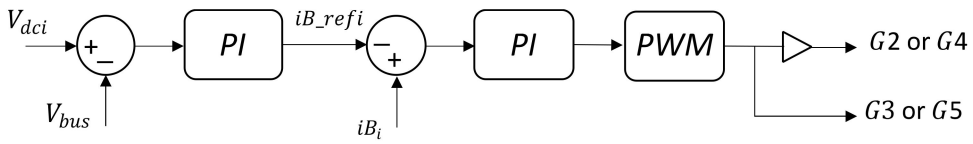

Figure 6. Bidirectional DC-DC control diagram (Buck–Boost).

3.2. Droop (V-P) Controller Design in Batteries

The voltage droop control by the conventional method has presented favorable results in MG-DC by orienting the power distribution according to the variation in the available capacity in each source. Considering a unidirectional or bidirectional voltage-controlled power electronic converter, the conventional droop method is expressed by Equation (3):

$$V_{dci} = V_{nom} - m_p \cdot P_{fci} \tag{3}$$

$$m_i = \frac{\Delta V_{\max}}{P_{\max i}} \tag{4}$$

$$\Delta V_{\max} = V_{nom} - V_{\min} \tag{5}$$

where V_{dci} is the output of the droop controller, V_{nom} is the nominal value of the microgrid, m_i is the droop coefficient, and P_{fci} is the power obtained at the output of the filter. m_i obtained by Equation (4) results from the maximum power in the battery $P_{\max_i}$ concerning the variation in the maximum acceptable voltage $\Delta V_{\max}$, and $\Delta V_{\max}$ is obtained by

Equation (5), where $V_{\min}$ is obtained from the difference between the nominal voltage and 5% of the nominal voltage V_{nom}.

As can be seen in Figure 3 the output of the droop control (V_{dci}) modifies the reference voltage of the local controller to distribute power between the batteries when operating in discharge mode.

As shown in Figure 2, the ESSs are connected in parallel, and it is essential to distribute the power according to each unit's SOC and capacity. Usually, the output power is inversely proportional to the droop coefficient, and by selecting a value to the droop coefficient that is inversely proportional to the SOC, the output power of each converter will be proportional to each SOC. Ideally, the storage unit with a higher SOC will deliver higher power versus a storage unit with a lower SOC, which will deliver a lower power.

The primary control strategies produce a voltage deviation, so a secondary control is necessary. The secondary control oversees restoring the voltage to MG-DC nominal values and managing the batteries' operation, respecting their capacities. The description of the secondary control design is detailed in the following section.

4. Distributed Secondary Controller for Efficient Battery Management

Although the droop controller implemented in the batteries (Equation (3)) allows power sharing between the units, to achieve this objective, the voltage of each battery is modified; therefore, the voltage on the DC bus presents deviations. So, it is necessary to implement an extra control loop called secondary control, which is responsible for restoring the global variables of the system to their nominal value, but because there is a tradeoff between restoring voltage and active power sharing to implement a traditional secondary control based on a voltage restorer that causes a negative effect on the power sharing in the batteries, which is shown as a deterioration in its life mainly in those of lower capacity because they will present greater charge and discharge cycles. To overcome this issue, in this research, a distributed secondary control is proposed. The controller meets two control objectives, the first one is to restore voltage and the second one is to share active power between the batteries respecting their capacities. Figure 3 at the top shows the architecture of the proposed secondary control, where a PI controller is implemented to restore the voltage with a traditional approach (Ψ_i). In addition, to guarantee active power sharing between the batteries respecting their capacities, a PI controller based on consensus theory [32] is integrated where the common objective is to share power (ξ_i). These two control actions add up (λ_i) and cause a change in the primary droop which in turn is shown in the local controls.

The distributed control architecture allows the control effort to be distributed in all the dispatchable units of an MG. This type of architecture has a communication network where each unit has at least one link line, so that information can be shared among all units, which has allowed the implementation of consensus-based control algorithms [13].

Under this control architecture, applications have been realized as a distributed secondary control for MG AC MG-AC, where the consensus objective is to restore frequency and share active power between all generating units [33]. In addition, applications have been made to mitigate imbalances for three-phase three-wire isolated microgrids (MG) [34]. For share imbalance and harmonics problems, distributed control strategies in MG-AC are also used [35], as well as mining-industry microgrid applications [36]. In more complex applications, a distributed control strategy for frequency control, congestion management, and optimal dispatch (OD) in isolated AC microgrids has been proposed [37]. These works are applications to MG-AC, and do not consider storage units. Thanks to the distributed control architecture, consensus algorithms can be implemented; the general description is shown below.

Consider the graph $G = (N, E, A)$, where N is the set of vertices, $N = \{1, \ldots, n\}$ represents the DG units in the microgrid, E represents the set of edges of the communication links $(i, j) \in E$, and A is the adjacency matrix $n \times n$ of the graph G. A is a symmetric matrix

with elements $a_{ij} = a_{ji} \geq 0$. If the node i receives information from the node j, then $E(i,j) = 1$ and $a_{ij} = 1$, otherwise $a_{ij} = 0$.

Let us suppose that information flows between the vertices i and j. Consensus on the x variable is said to be achieved if $x_i(t) - x_j(t) \to 0$, and this consensus is achieved according to the first-order consensus shown in Equation (6) [32]:

$$\dot{x}_i = -\sum_{j \in Nj \neq i} a_{ij}(x_i - x_j) \tag{6}$$

Figure 7 shows a communication network topology in a distributed control architecture; it can be seen that each node has at least one communication line, and the matrix A represents the fact that the connection between nodes is made up of a_{ij} elements, where i is the local node and j the neighboring node. As can be seen in the matrix A, those nodes that are not connected have a value of zero. This communication matrix is dynamic, meaning if any node x is disconnected, it can change its state to a value of zero. In this research, each represents a battery [13].

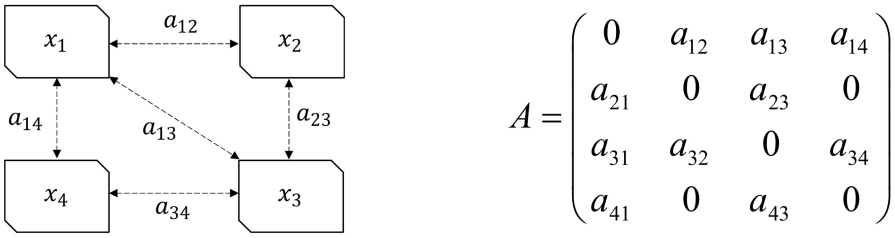

Figure 7. Example of a graph of four agents and their associated adjacency matrix. Developed from [38].

Distributed Control Design

The proposed distributed secondary control (λ_i) defined by Equation (7) fulfills two control objectives, the first one restoring the (Ψ_i) voltage, and the second one distributing power respecting the capacity of the (ξ_i) batteries.

In the primary control Equation (3), a second control action (λ_i) is added, and the modified droop equation is shown in (8):

$$\lambda_i = \Psi_i + \xi_i \tag{7}$$

$$V_{dci} = V_{nom} - m_i \cdot P_{fci} + \lambda_i \tag{8}$$

The voltage restoration control (Ψ_i) is based on a traditional secondary control strategy that aims to correct the voltage deviations caused by the primary control (Figure 3) where a nominal voltage V_{nom} required on the DC bus is compared with a droop voltage V_{dci}. The error is corrected through a PI controller (Figure 8) where it maintains a constant voltage on the DC bus.

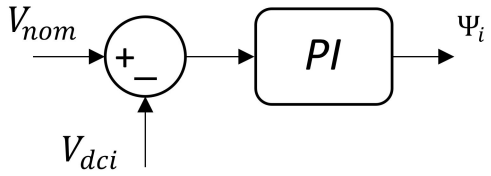

Figure 8. Distributed secondary control diagram for voltage restoration.

The action to restore voltage is defined by Equation (9), which considers tuning the gains of the control K_p, which is the proportional gain, and K_i, which is integral gain;

in turn, this controller can be rewritten as in Equation (10), where K_T is the joint gain of $K_p + K_i$:

$$\Psi_i = K_p(V_{nom} - V_{dci}) + K_i \int (V_{nom} - V_{dci}) \tag{9}$$

$$\dot{\Psi}_i = K_T(V_{nom} - V_{dci}) \tag{10}$$

This controller is efficient regarding voltage regulation on the DC bus. However, the restoring voltage produces an inadequate power sharing as the capacities of each unit are not respected, i.e., the lower capacity battery has a higher number of duty cycles and, therefore, an accelerated degradation.

To correct the power sharing among batteries while respecting the voltage restoration, the controller in (ξ_i) is included in (λ_i) based on the consensus algorithms described in Equation (11). Its specific design is presented in Figure 9, where ξ_i is the control action generated by the PI controller described in Equation (11). This control action is incorporated into the control levels already described (Figure 3), in which (11) can be rewritten as Equation (12), where $K_t = K_p + K_i$.

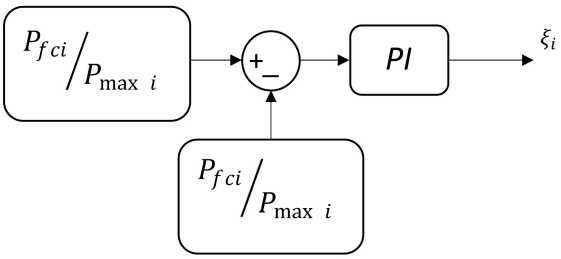

Figure 9. Centralized secondary control diagram.

As can be noticed, the process is represented by the summation that seeks the power in a unit that is equal to the power of its neighbors, but it respects its capacity, so its maximum power is added to each power in its denominator. In Equation (12), i represents the battery where the algorithm is being programmed, while j is the neighbor battery, $P_{\max i}$ represents the maximum power in the battery, and i and a_{ij} are the elements of the adjacency matrix that takes a value of one if there is a connection and zero if there is no communication line.

$$\xi_i = -K_p \sum_{j\in N, j\neq i} a_{ij}\left(\frac{P_{fci}}{P_{\max\ i}} - \frac{P_{fcj}}{P_{\max\ j}}\right) - K_i \int \sum_{j\in N, j\neq i} a_{ij}\left(\frac{P_{fci}}{P_{\max\ i}} - \frac{P_{fcj}}{P_{\max\ j}}\right) \tag{11}$$

$$\dot{\xi}_i = -\sum_{j\in N, j\neq i} a_{ij}\left(\frac{P_{fci}}{P_{\max\ i}} - \frac{P_{fcj}}{P_{\max\ j}}\right)(K_t) \tag{12}$$

Figure 10 shows the flowchart on the Distributed Secondary Controller for an Efficient Battery, which is based on voltage restoration and power sharing. In secondary control development, it is necessary to implement and design the primary control (conventional droop control) to modify the reference voltage. In the first instance, the values of the primary control are evaluated and incorporated in the distributed control in order to have a communication link between the storage units. When evaluating the voltage on the DC bus, it should remain in the 48 V regime, which allows the analysis of the appropriate power sharing; otherwise, if this factor is not complied with, a control action based on a consensus algorithm ξ_i is added to compensate for this power deviation. If the voltage does not remain in the 48 V regime, a control action is incorporated Ψ_i to allow voltage regulation; when this parameter is satisfied, it is checked if the power is distributed correctly according to its capacities. Since it does not have a correct power distribution, a control action λ_i, which is the joint value of the regulatory action Ψ_i, and a consensus algorithm ξ_i is incorporated.

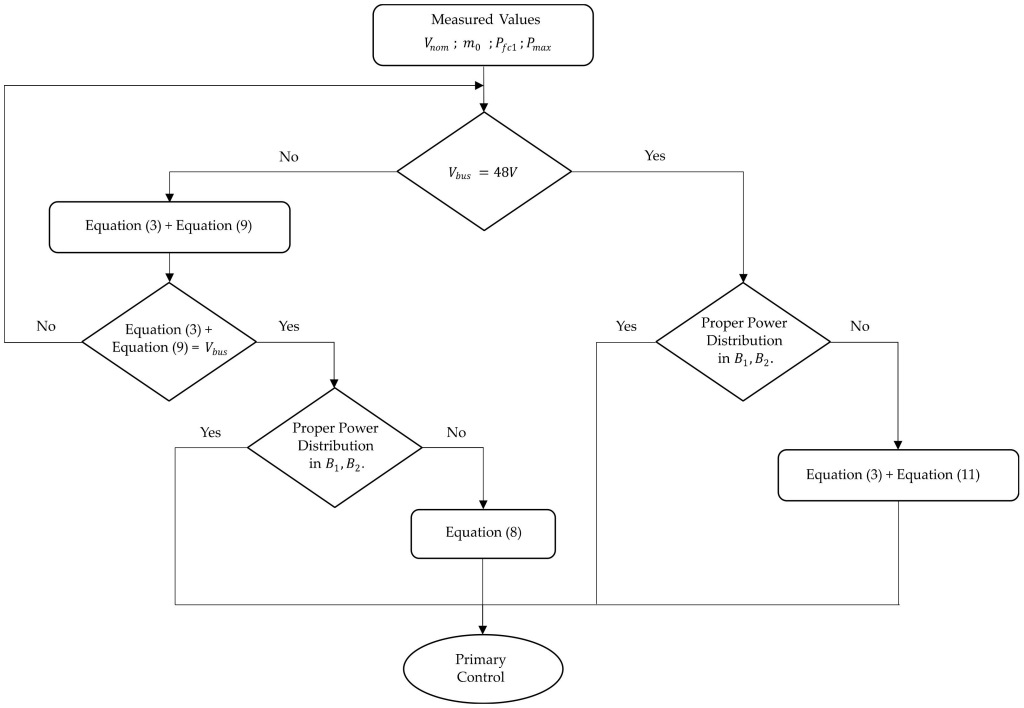

Figure 10. Flow chart for Distributed Secondary Controller for Efficient Battery Management.

5. Results

For the validation of the efficient management of the storage units, a distributed control scheme based on a consensus algorithm is proposed. An isolated MG-DC was considered, consisting of storage units and a generation unit which were designed and modeled using MATLAB/Simulink by simulation; the system consisted of a PV and two batteries of different capacities connected in parallel to a DC bus, which supplied the demand to a load. It is worth mentioning that the storage units' full charge and discharge response would take several hours; however, to verify the charge and discharge cycles, the operating range of the SOC was restricted. Therefore, the simulated results were run for 155 s, with a smooth transition from a cloudy to clear sky, meaning the loading and unloading of the ESS could be appreciated for further analysis based on the SOC. The controllers were subjected to different radiation scenarios to verify the correct and efficient operation of charging and discharging the batteries. The analysis was performed using batteries with different capacities that allowed us to visualize the appropriate charge distribution according to the different capacities without overcharging the battery with a lower capacity. The system parameters for both the batteries and the PV are shown in Tables 1 and 2, respectively. The parameters of the converters, A, B1, B2, filters, and load are given in Table 3.

Table 1. Battery 1 and 2 parameters.

Description	Parameter	Battery 1	Battery 2
Nominal Voltage	V	36 V	36 V
Nominal Capacity	Ah	50 Ah	6.5 Ah
Initial Charge State	SOC (%)	50%	50%

Table 2. Photovoltaic panel parameters.

Description	Parameter	Value
Array tension panel	V_{oc}	36.3 V
Array current panel	I_{sc}	7.84 A
Max. Power array tension	V_{mpp}	29 V
Max. Power array current	I_{mpp}	7.35 A

Table 3. Characteristics of the converters.

Description		Parameter	Value
Inductance at PV		L_{pv}	5×10^{-3} H
Battery Inductance 1		L_{bat1}	5×10^{-3} H
Battery Inductance 2		L_{bat2}	5×10^{-3} H
PV Capacitor		C_{pv}	100×10^{-6} H
DC Capacitor		C_{DC}	3300×10^{-6} H
Capacitor Battery 1		C_{bat1}	1000×10^{-6} H
Capacitor Battery 2		C_{bat2}	1000×10^{-6} H
Load	Voltage nominal	V_n	48 V
	Active power	P_L	1000 W

This section analyzes the performance of the three control levels (Figure 3), the local control, the primary control, and finally, the proposed secondary control. The efficient management of the ESS in an isolated MG-DC was analyzed, and it was verified that the power balance was fulfilled at all times in the MG-DC.

5.1. Power Balance

The power balance was analyzed considering that, regardless of the generation and load units, the power generated will always be equivalent to the power consumed, ensuring the system's stability; its equation can be represented as (13):

$$P_{pv} + P_{B1} + P_{B2} = P_L \tag{13}$$

where P_{pv} is the power of the photovoltaic panel and P_{B1} and P_{B2} are the power received or injected by the batteries. Equation (13) can be rewritten according to the operating state of the ESS, shown in the sign. When the battery operates in discharge mode, it injects or delivers power to the MG-DC (Boost mode) and its sign is positive, and when the batteries operate in charge mode, they consume energy (Buck mode) and its sign is negative, whereby P_L is the power demanded to supply the MG-DC load.

The power balance must be met at all control levels; however, how it is met may change depending on the control level and architecture.

5.2. Primary Control (Local Control and Conventional Droop Control)

To study the conventional droop control, several parameters were determined, such as a DC load, a nominal voltage of 48 V, and an operating voltage variation of approximately 5% for each source, whereby a value of 2.4 V was consequently established, and the calculation of the maximum power of the battery was performed. This led us to obtain the droop coefficient, which was expressed in minimum values of 0.0013 for battery 1 and 0.01 for battery 2. Figure 11 shows an irradiation profile used for the photovoltaic panel in a specific time interval. Figure 12a shows the power distribution to supply the demand (red line), where it was determined that battery 1 (green line) delivered more power because of

its higher capacity compared with battery 2 (purple line) with a lower capacity. Therefore, with this premise, it was demonstrated that the power distribution was adequate since no battery was demanded or competed for the higher distribution; this could also be verified with the behavior of the SOC in Figure 12b, where its discharge was proportional to the delivered power that differed in a slight value, whereby the purpose of implementing the droop concept was the adjustment between load sharing. However, this task became a tradeoff with the voltage control in the MC-DC, as shown in Figure 13, where the voltage was stabilized at the Set Point (SP); therefore, although there was reasonable control, this did not remain constant at its nominal reference value, so this method was deficient. Therefore, to compensate for the voltage deviation on the DC bus, we implemented a control action (Ψ_i), which was responsible for restoring the voltage.

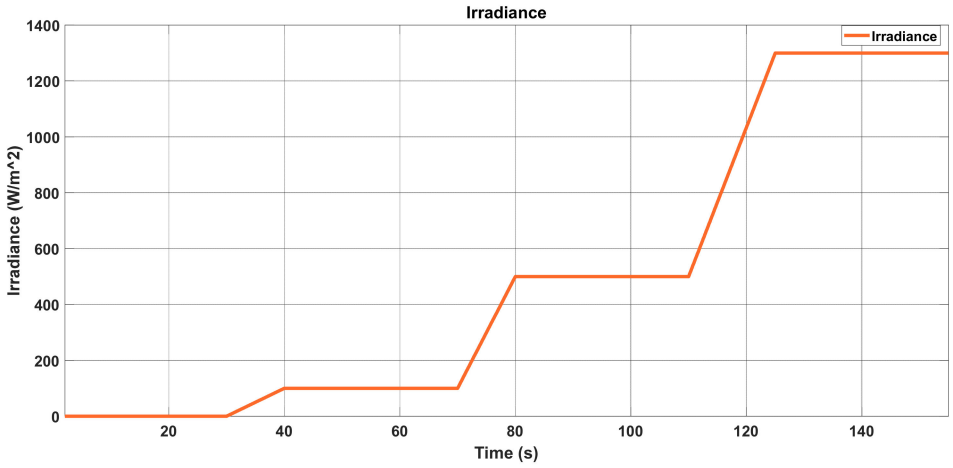

Figure 11. Irradiance profile.

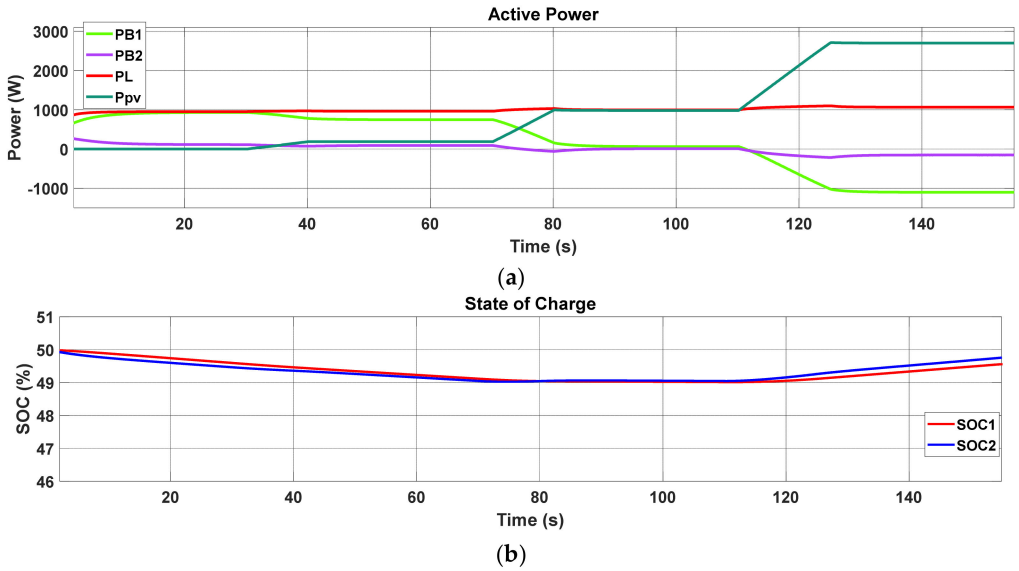

Figure 12. Conventional droop control, (**a**) system power sharing and (**b**) SOC in batteries 1 and 2 at a time of 155 s.

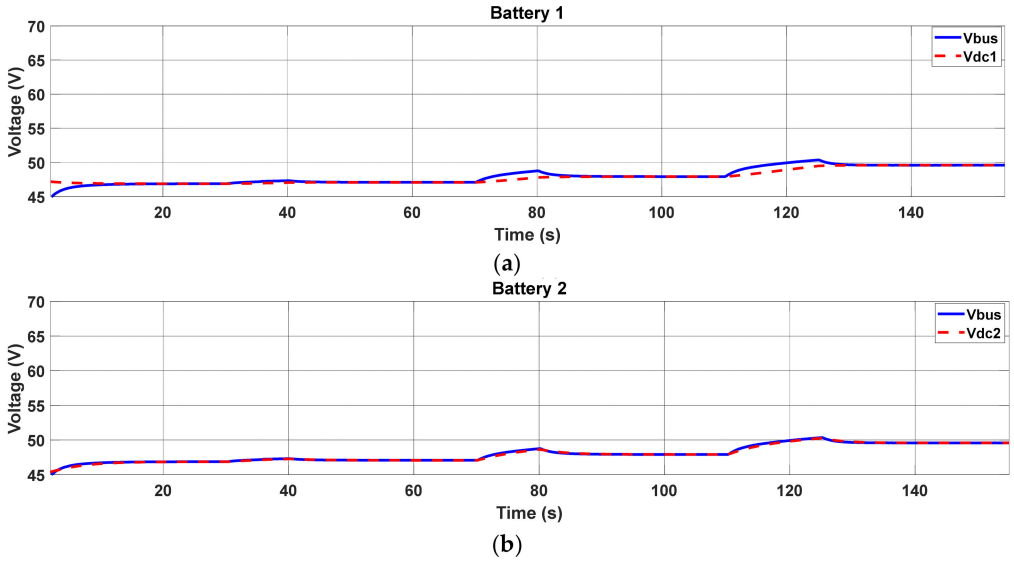

Figure 13. DC bus voltage control with conventional droop for (**a**) battery 1 and (**b**) battery 2 at a time of 155 s.

5.3. Distributed Secondary Control

The objective was to correct the voltage deviation of the conventional droop control by incorporating a traditional distributed secondary control that considers only voltage restoration. Figure 3 shows that the battery converters connected in parallel were controlled by a conventional droop function, and subsequently a voltage control action (Ψ_i) was designed and implemented in the droop function of Equation (3) at the main control level. Figure 14 shows the performance of the traditional secondary controller to restore the voltage, where the voltage problem that was the deviation from the nominal value on the DC bus produced by the primary control was compensated (Figure 13). However, by incorporating this control, the battery powers were not adequately distributed (Figure 15a), and it was found that the power in battery 1 (green line) was similar to the power delivered through battery 2 (purple line) even though they were of different capacities. This could also be validated in the SOC analysis in Figure 15b, where it shows a hurried discharge of the lower capacity battery 2 versus a slow discharge of the higher capacity battery 1, which induced a higher number of duty cycles of the lower capacity battery, degrading it in an accelerated way. Therefore, this method was deficient, and to compensate for the power distribution in the MG-DC, a control action was implemented with a consensus algorithm (ξ_i) that oversaw restoring the powers.

5.4. Distributed Control Based on a Consensus Algorithm

The power bad distribution limitations at the DC load supply were corrected by incorporating the power compensation component in the distributed secondary control based on a consensus algorithm. This method ensured that the batteries distributed their power according to the parameters that characterized each battery. Figure 3 shows that the converters connected in parallel were controlled by a conventional droop function together with a secondary control; then, a distributed control action was designed based on a consensus algorithm ξ_i, which was implemented in the droop function at the primary control level. Figure 16a shows the appropriate power distribution for each storage unit, verifying that the unit with a higher capacity delivered a higher power (green line) and the unit with a lower capacity provided a lower power (purple line). The SOC of the ESS presented a minimum deviation between the two batteries in their discharged state; this means that the two batteries experienced a similar discharge condition regardless of their capacities, which made the batteries degrade equally (Figure 16b). While in the charging mode, the lower-capacity battery presented a sharing adequate to its capacities, i.e., its

charge was faster (Figure 16b). An efficient MG-DC's performance in preserving battery life was validated.

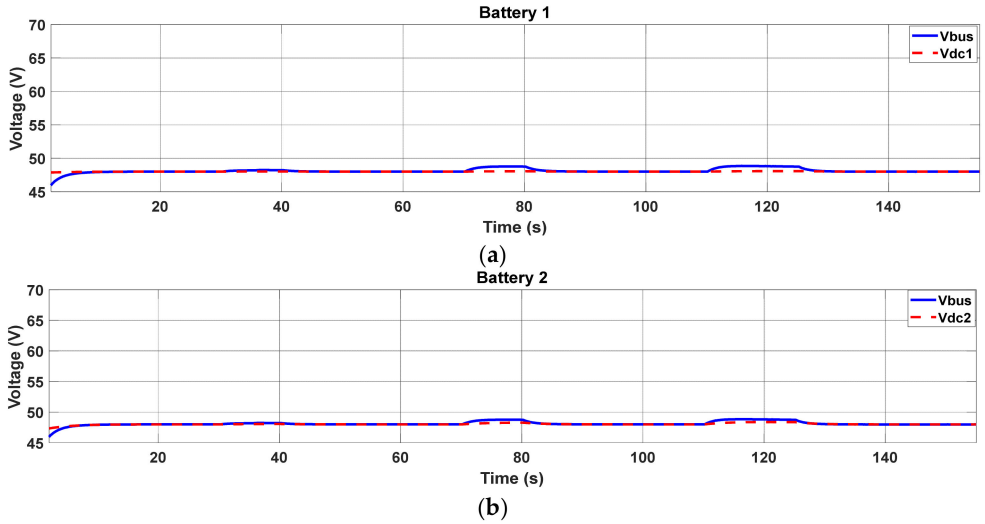

Figure 14. DC bus voltage control with distributed secondary control for voltage restoration for (**a**) battery 1 and (**b**) battery 2 in a time of 155 s.

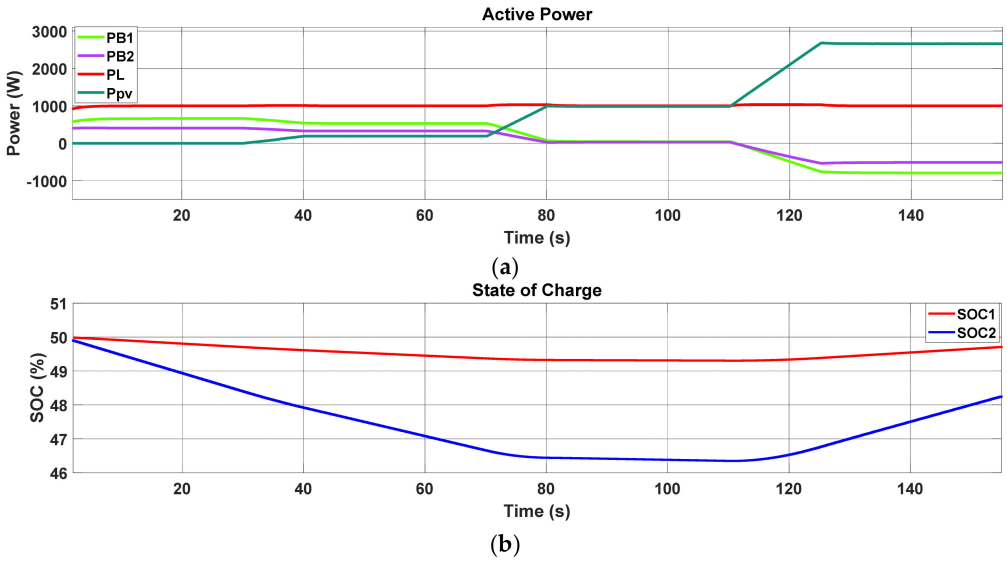

Figure 15. Distributed secondary control for voltage restoration, (**a**) system power sharing and (**b**) SOC in batteries 1 and 2 in a time of 155 s.

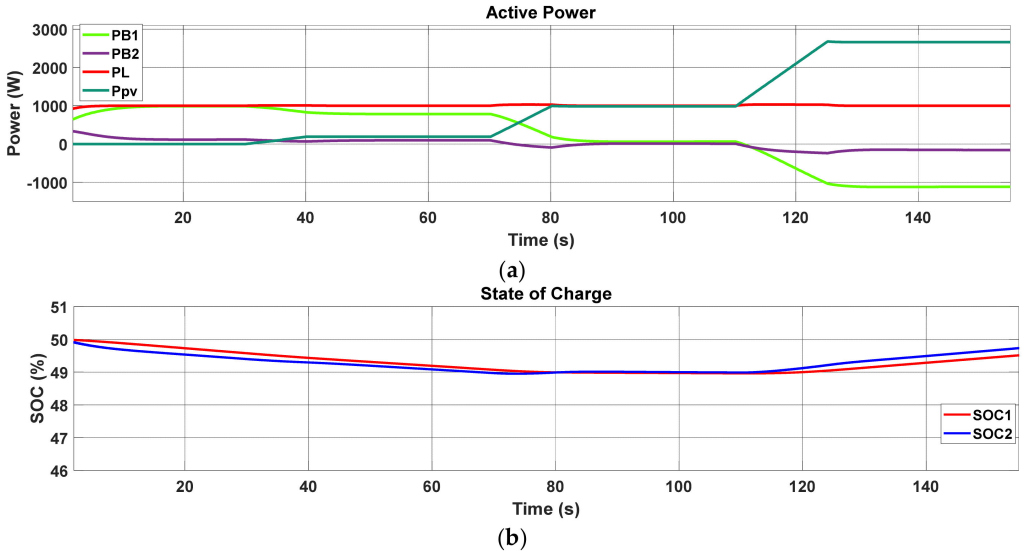

Figure 16. Distributed secondary control based on consensus algorithm, (**a**) system power sharing and (**b**) SOC in batteries 1 and 2 in a time of 155 s.

Figure 17 shows the results of the voltage control for the distributed secondary control integrating a consensus algorithm, where the DC bus voltage maintained its stable values in the SP, with overshoot values of 0.76% at different time intervals. Therefore, the voltage restoration and power sharing were effectively achieved.

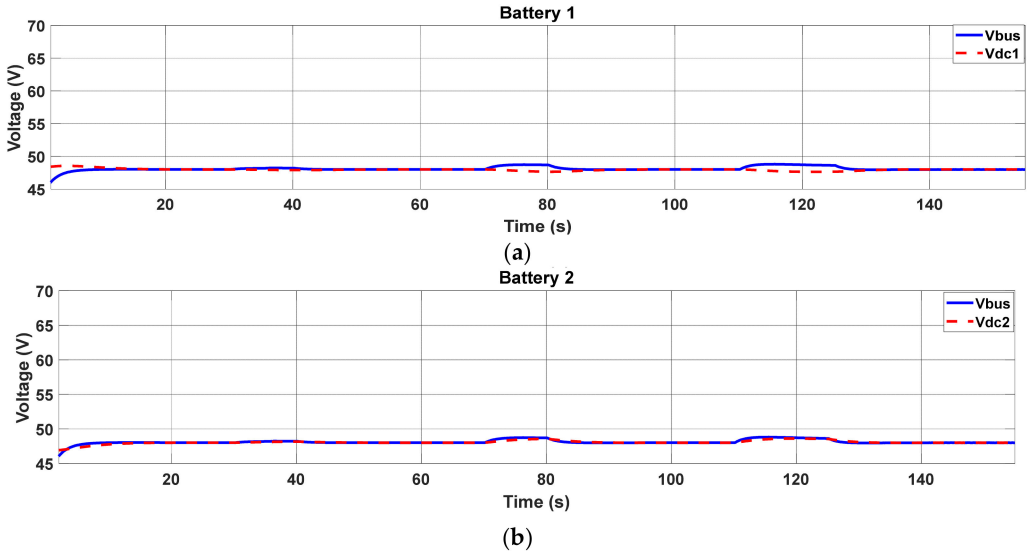

Figure 17. DC bus voltage control with distributed secondary control based on consensus algorithm for (**a**) battery 1 and (**b**) battery 2 in a time of 155 s.

6. Conclusions

To ensure the efficient management of an isolated MG-DC with storage units oriented toward power sharing respecting the capacities of each battery, this research proposes a distributed secondary control based on a consensus algorithm to avoid the gradual deterioration of the storage units of different capacities. To ensure power distribution and a nominal operating voltage, as well as stability in the DC bus, a control architecture composed of three levels was proposed for the efficient management of the MG; the first one corresponded to the local control of the current and voltage for the operation in charge and discharge mode of the batteries, while for the photovoltaic generator, an

MPPT control based on the P & O technique was incorporated to take full advantage of the available solar resource. The second level of control corresponded to a voltage drop control which modified the reference voltage of the local controller to share power between the batteries. However, the voltage on the DC bus differed from the nominal voltage, and the power in the local load was affected, causing the power distribution in the load to not be constant. Finally, to compensate for this deviation, a secondary voltage restoring control action (Ψ_i) was included; although it acted as a correct voltage regulator in the DC bus, it did not distribute the power properly because the batteries, regardless of their capacity, dispatched energy uniformly, attributing to the accelerated degradation of the lower-capacity battery. Based on this analysis, a distributed secondary control was integrated based on a consensus algorithm (ξ_i) that allowed the efficient distribution of power by batteries of different capacities. The advantages and impact of the proposed distributed secondary control based on a consensus algorithm were the correct voltage control in the DC bus, significantly reducing the voltage variations presented in the primary control. The power distribution was according to the characteristics of each battery so that a battery with a lower capacity would deliver less power compared with a battery with a higher capacity showing a simultaneous discharge in the two units; this relationship was established by the efficient behavior of the SOC while efficiently managing the MG, which preserved the life of the batteries.

Author Contributions: Conceptualization, A.P.M., P.J.P. and J.R.L.; methodology, A.P.M., P.J.P., J.R.L., D.O.-V. and C.B.; software, A.P.M. and P.J.P.; validation, A.P.M., P.J.P. and J.R.L.; formal analysis, A.P.M., P.J.P., J.R.L., D.O.-V. and C.B.; investigation, A.P.M. and P.J.P.; resources, J.R.L.; data curation, A.P.M., P.J.P. and J.R.L.; writing—original draft preparation, A.P.M., P.J.P., J.R.L. and D.O.-V.; writing—review and editing, A.P.M., P.J.P., J.R.L., D.O.-V. and C.B.; visualization, A.P.M., P.J.P. and J.R.L.; supervision, J.R.L., D.O.-V. and C.B.; project administration, J.R.L.; funding acquisition, J.R.L. All authors have read and agreed to the published version of the manuscript.

Funding: This research received no external funding.

Data Availability Statement: Not applicable.

Acknowledgments: This work was supported in part by the Universidad de las Fuerzas Armadas ESPE and KU Leuven through the Project "MIRA-ESTE: Specific, Innovative Microgrids Solutions (Accounting for Environmental, Social, Technological and Economic Aspects) for isolated rural areas of Ecuador" under the Project 2020-EXT-007, and in part by the Vlaamse Interuniversitaire Raad (VLIR)—Universitaire Ontwikkelingssamenwerking (UOS) and the Belgium Development Cooperation (DGD) through the Project EC2020SIN322A101. In addition, the authors would like to thank the Subdirección de Redes, Estrategia y Conocimiento (REC), Agencia Nacional de Investigación y Desarrollo (ANID) through the Chilean Grant: ANID—concurso de fomento a la vinculación internacional para instituciones de investigación regionales (modalidad corta duración)—FOVI210023.

Conflicts of Interest: The authors declare no conflict of interest.

Nomenclature

A	Adjacency matrix
a_{ij}	Elements of the adjacency matrix (i is the local node and j is the neighboring node)
Ah	Nominal Capacity
$C_{bat1}; C_{bat2}$	Batteries Capacitor
C_{DC}	DC Capacitor
C_{pv}	PV Capacitor
D	Duty cycle
$D(k)$	Current duty cycle
$D(k-1)$	Previous duty cycle
E	Set of edges of the communication links
G	Graph of the communication links
$G_1; G_2; G_3; G_4; G_5$	Converter gates
i	Storage unit

iB_ref_i	Reference current output of the PI control
iB_i	Battery current
I_{mmp}	Max. power array current
I_{pv}	Photovoltaic current
I_{SC}	Array current panel
K_i	Integral gain
K_p	Proportional gain
K_T	Joint gain of proportional gain and integral gain for voltage regulator
K_t	Joint gain of proportional and integral gain for the consensus-based algorithm
$L_{bat1}; L_{bat1}$	Batteries inductance
L_{pv}	Inductance at PV
m_i	Droop coefficient
N	Set of vertices
$P_{B1}; P_{B2}$	Battery power
P_{fci}	Power obtained at the output of the filter
P_L	Power demanded to supply the MG-DC load
$P_{\max i}$	Represents the maximum power in the battery
P_{pv}	Photovoltaic power
$P_{pv}(k-1)$	Photovoltaic power in a previous instant
V	Nominal voltage batteries
V_{bus}	Reference voltage on the DC bus
V_{dci}	Output of the droop controller
V_{min}	Acceptable minimum voltage
V_n	Voltage nominal Load
V_{nom}	Nominal value of the microgrid
V_{OC}	Array tension panel
V_{pv}	Photovoltaic voltage
$V_{pv}(k-1)$	Photovoltaic voltage in a previous instant
x	Represents the battery in a communication link
ΔD	Perturbation around the duty cycle
ΔV_{max}	Variation in the maximum acceptable voltage
Ψ_i	PI controller is implemented to restore the voltage with a traditional approach
ξ_i	PI controller based on consensus theory
λ_i	Joint value of regulatory action and a consensus algorithm
$DESUs$	Distributed energy storage units
DG	Distributed generation
EMS	Energy management system
ESS	Energy storage system
$FO-PID$	Fractional order proportional integral derivative
$MG-AC$	AC microgrid
$MG-DC$	DC microgrid
$MPPT$	Maximum power point tracking
OD	Optimal dispatch
PID	Control proportional integral derivative
PV	Photovoltaic
PWM	Pulse width modulation
$P\ \&\ O$	Perturb and observe
RES	Renewable energy sources
SOC	State of charge
SP	Set point
TS	Takagi–Sugeno

References

1. Cervantes Leopoldo, X.G. La Generación Distribuida y las Fuentes Renovables de energía en el Ecuador Distributed Generation and Renewable Sources of energy in Ecuador Geração Distribuída e Fontes Renováveis de Energia no Equador. *Dom. Cien.* **2021**, *7*, 884–895.
2. Ullah, Z.; Elkadeem, M.; Kotb, K.M.; Taha, I.B.; Wang, S. Multi-criteria decision-making model for optimal planning of on/off grid hybrid solar, wind, hydro, biomass clean electricity supply. *Renew Energy* **2021**, *179*, 885–910. [CrossRef]

3. Chen, Y.; Xu, P.; Gu, J.; Schmidt, F.; Li, W. Measures to improve energy demand flexibility in buildings for demand response (DR): A review. *Energy Build.* **2018**, *177*, 125–139. [CrossRef]
4. Carrión, D.; Ortiz, L. Generación distribuida a partir de bicicletas estáticas y sistemas híbridos. *Ingenius* **2013**, 44–48. [CrossRef]
5. Pata, U.K. Linking renewable energy, globalization, agriculture, CO2 emissions and ecological footprint in BRIC countries: A sustainability perspective. *Renew. Energy* **2021**, *173*, 197–208. [CrossRef]
6. Chen, C.; Pinar, M.; Stengos, T. Determinants of renewable energy consumption: Importance of democratic institutions. *Renew. Energy* **2021**, *179*, 75–83. [CrossRef]
7. Rodriguez, M.; Espin, V.; Arcos-Aviles, D.; Martinez, W. Energy management system for an isolated microgrid based on Fuzzy logic control and meta-heuristic algorithms. In Proceedings of the 2022 IEEE 31st International Symposium on Industrial Electronics (ISIE), Anchorage, AK, USA, 1–3 June 2022.
8. Yépez, H.; Yépez, D. Control de Modo Deslizante Para Microrredes: Una Revisión. *Investig. Tecnológica IST Cent. Técnico* **2020**, *2*, 14.
9. Arcos-Aviles, D.; Pascual, J.; Guinjoan, F.; Marroyo, L.; Sanchis, P.; Marietta, M.P. Low complexity energy management strategy for grid profile smoothing of a residential grid-connected microgrid using generation and demand forecasting. *Appl. Energy* **2017**, *205*, 69–84. [CrossRef]
10. Dulce Mera, F.A. Modelamiento y Control de Una Microrred en Modo Isla. Master's Thesis, Universidad de los Andes, Bogotá, Colombia, June 2015.
11. Rodriguez, M.; Arcos-Aviles, D.; Llanos, J.; Salazar, A.; Guinjoan, F.; Motoasca, E.; Martinez, W. Fuzzy-based energy management system for isolated microgrids using generation and demand forecast. In Proceedings of the 2021 23rd European Conference on Power Electronics and Applications, EPE 2021 ECCE Europe, Ghent, Belgium, 6–10 September 2021; pp. 1–10.
12. Arcos-Aviles, D.; Pascual, J.; Marroyo, L.; Sanchis, P.; Guinjoan, F. Fuzzy Logic-Based Energy Management System Design for Residential Grid-Connected Microgrids. *IEEE Trans. Smart Grid* **2016**, *9*, 530–543. [CrossRef]
13. Espina, E.; Llanos, J.; Burgos-Mellado, C.; Cardenas-Dobson, R.; Martinez-Gomez, M.; Saez, D. Distributed Control Strategies for Microgrids: An Overview. *IEEE Access* **2020**, *8*, 193412–193448. [CrossRef]
14. Garcés, A. Small-signal stability analysis of DC microgrids considering electric vehicles. *Rev. Fac. Ing.* **2018**, *2018*, 1–7. [CrossRef]
15. Bayrak, G.; Ghaderi, D. An improved step-up converter with a developed real-time fuzzy-based MPPT controller for PV-based residential applications. *Int. Trans. Electr. Energy Syst.* **2019**, *29*, e12140. [CrossRef]
16. Rao, C.; Hajjiah, A.; El-Meligy, M.A.; Sharaf, M.; Soliman, A.T.; Mohamed, M.A. A Novel High-Gain Soft-Switching DC-DC Converter with Improved P&O MPPT for Photovoltaic Applications. *IEEE Access* **2021**, *9*, 58790–58806. [CrossRef]
17. Das, M.; Agarwal, V. Novel High-Performance Stand-Alone Solar PV System with High-Gain High-Efficiency DC–DC Converter Power Stages. *IEEE Trans. Ind. Appl.* **2015**, *51*, 4718–4728. [CrossRef]
18. Abdel-Rahim, O.; Wang, H. Aswan University a New High Gain DC-DC Converter with Model-Predictive-Control Based MPPT Technique for Photovoltaic Systems. *CPSS Trans. Power Electron. Appl.* **2020**, *5*, 191–200. [CrossRef]
19. Romero Andrade, G.D. Optimización del Proceso de Carga y Descarga de Bancos de Baterías en Sistemas de Generación Fotovoltaica. Bachelor's Thesis, Universidad Politécnica Salesiana, Quito, Ecuador, August 2018.
20. Rezk, H.; Nassef, A.M.; Abdelkareem, M.A.; Alami, A.H.; Fathy, A. Comparison among various energy management strategies for reducing hydrogen consumption in a hybrid fuel cell/supercapacitor/battery system. *Int. J. Hydrogen Energy* **2019**, *46*, 6110–6126. [CrossRef]
21. Al Alahmadi, A.A.; Belkhier, Y.; Ullah, N.; Abeida, H.; Soliman, M.S.; Khraisat, Y.S.H.; Alharbi, Y.M. Hybrid Wind/PV/Battery Energy Management-Based Intelligent Non-Integer Control for Smart DC-Microgrid of Smart University. *IEEE Access* **2021**, *9*, 98948–98961. [CrossRef]
22. Belal, E.K.; Yehia, D.M.; Azmy, A.M. Adaptive droop control for balancing SOC of distributed batteries in DC microgrids. *IET Gener. Transm. Distrib.* **2019**, *13*, 4667–4676. [CrossRef]
23. Baharizadeh, M.; Golsorkhi, M.S.; Shahparasti, M.; Savaghebi, M. A Two-Layer Control Scheme Based on *P*—*V* Droop Characteristic for Accurate Power Sharing and Voltage Regulation in DC Microgrids. *IEEE Trans. Smart Grid* **2021**, *12*, 2776–2787. [CrossRef]
24. Xing, L.; Xu, Q.; Guo, F.; Wu, Z.-G.; Liu, M. Distributed Secondary Control for DC Microgrid With Event-Triggered Signal Transmissions. *IEEE Trans. Sustain. Energy* **2021**, *12*, 1801–1810. [CrossRef]
25. Xing, L.; Mishra, Y.; Guo, F.; Lin, P.; Yang, Y.; Ledwich, G.; Tian, Y.-C. Distributed Secondary Control for Current Sharing and Voltage Restoration in DC Microgrid. *IEEE Trans. Smart Grid* **2019**, *11*, 2487–2497. [CrossRef]
26. Lu, X.; Sun, K.; Guerrero, J.M.; Vasquez, J.C.; Huang, L. State-of-Charge Balance Using Adaptive Droop Control for Distributed Energy Storage Systems in DC Microgrid Applications. *IEEE Trans. Ind. Electron.* **2013**, *61*, 2804–2815. [CrossRef]
27. Xu, D.; Xu, A.; Yang, C.; Shi, P. A Novel Double-Quadrant SoC Consistent Adaptive Droop Control in DC Microgrids. *IEEE Trans. Circuits Syst. II Express Briefs* **2019**, *67*, 2034–2038. [CrossRef]
28. Papadimitriou, C.N.; Zountouridou, E.I.; Hatziargyriou, N.D. Review of hierarchical control in DC microgrids. *Electr. Power Syst. Res.* **2015**, *122*, 159–167. [CrossRef]
29. Dahale, S.; Das, A.; Pindoriya, N.M.; Rajendran, S. An overview of DC-DC converter topologies and controls in DC microgrid. In Proceedings of the 2017 7th International Conference on Power Systems, ICPS 2017, Pune, India, 21–23 December 2017; pp. 410–415. [CrossRef]

30. Hichem, L.; Leila, M.; Amar, O. *Comparative Study of Perturb-and-Observe and Fuzzy Logic MPPT for Stand-Alone PV System*; Springer International Publishing: Berlin/Heidelberg, Germany, 2022; Volume 361. [CrossRef]
31. Islam, F.R.; Prakash, K.; Mamun, K.A.; Lallu, A.; Mudliar, R. Design a Optimum MPPT Controller for Solar Energy System. *Indones. J. Electr. Eng. Comput. Sci.* **2016**, *2*, 545. [CrossRef]
32. Simpson-Porco, J.W.; Shafiee, Q.; Dörfler, F.; Vasquez, J.C.; Guerrero, J.M.; Bullo, F. Secondary Frequency and Voltage Control of Islanded Microgrids via Distributed Averaging. *IEEE Trans. Ind. Electron.* **2015**, *62*, 7025–7038. [CrossRef]
33. Llanos, J.; Gomez, J.; Saez, D.; Olivares, D.; Simpson-porco, J. Economic Dispatch by Secondary Distributed Control in Microgrids Economic Dispatch by Secondary Distributed Control in Microgrids Acknowledgments Keywords. In Proceedings of the 2019 21st European Conference on Power Electronics and Applications (EPE '19 ECCE Europe), Genova, Italy, 3–5 September 2019. [CrossRef]
34. Burgos-Mellado, C.; Donoso, F.; Llanos, J.; Martinez-Gomez, M.; Morales-Paredes, H.K.; Torres, M. Consensus-Based Distributed Control for Improving the Sharing of Unbalanced Currents in Three-Phase Three-Wire Isolated Microgrids. In Proceedings of the 2021 6th IEEE Workshop on the Electronic Grid (eGRID), New Orleans, LA, USA, 8–10 November 2021.
35. Burgos-Mellado, C.; Llanos, J.J.; Cardenas, R.; Saez, D.; Olivares, D.E.; Sumner, M.; Costabeber, A. Distributed Control Strategy Based on a Consensus Algorithm and on the Conservative Power Theory for Imbalance and Harmonic Sharing in 4-Wire Microgrids. *IEEE Trans. Smart Grid* **2019**, *11*, 1604–1619. [CrossRef]
36. Gomez, J.S.; Llanos, J.; Espina, E.; Burgos-Mellado, C.; Rodriguez, J. Cooperative Power Conditioners for Microgrids in Mining. In Proceedings of the 2021 23rd European Conference on Power Electronics and Applications (EPE'21 ECCE Europe), Ghent, Belgium, 6–10 September 2021. [CrossRef]
37. Llanos, J.; Olivares, D.E.; Simpson-Porco, J.W.; Kazerani, M.; Saez, D. A Novel Distributed Control Strategy for Optimal Dispatch of Isolated Microgrids Considering Congestion. *IEEE Trans. Smart Grid* **2019**, *10*, 6595–6606. [CrossRef]
38. Llanos Proaño, J.D.R. Design and Evaluation of Distributed Controllers for Optimal Dispatch and Congestion Management of Microgrids. Ph.D. Thesis, Universidad de Chile, Santiago de Chile, Chile, December 2020.